OPEN ACCESS
IOP Publishing
Journal of Physics: Condensed Matter
J. Phys.: Condens. Matter **34** (2022) 494002 (11pp)
https://doi.org/10.1088/1361-648X/ac9a1c

Kinetics of rapid growth and melting of $Al_{50}Ni_{50}$ alloying crystals: phase field theory *versus* atomistic simulations revisited*

Roberto E Rozas[1], Vladimir Ankudinov[2] and Peter K Galenko[3,4,]**

[1] Department of Physics, University of Bío-Bío, Av. Collao 1202, PO Box 5-C, Concepción, Chile
[2] Vereshchagin Institute of High Pressure Physics, Russian Academy of Sciences, 108840 Moscow (Troitsk), Russia
[3] Friedrich-Schiller-Universität Jena, Physikalisch-Astronomische Fakultät, D-07743 Jena, Germany
[4] Ural Federal University, Theoretical and Mathematical Physics Department, Laboratory of Multi-Scale Mathematical Modeling, 620000 Ekaterinburg, Russia

E-mail: peter.galenko@uni-jena.de

Received 21 May 2022, revised 16 August 2022
Accepted for publication 13 October 2022
Published 26 October 2022

Abstract

A revised study of the growth and melting of crystals in congruently melting $Al_{50}Ni_{50}$ alloy is carried out by molecular dynamics (MDs) and phase field (PF) methods. An embedded atom method (EAM) potential of Purja Pun and Mishin (2009 *Phil. Mag.* 89 3245) is used to estimate the material's properties (density, enthalpy, and self-diffusion) of the B2 crystalline and liquid phases of the alloy. Using the same EAM potential, the melting temperature, density, and diffusion coefficient become well comparable with experimental data in contrast with previous works where other potentials were used. In the new revision of MD data, the kinetics of melting and solidification are quantitatively evaluated by the 'crystal-liquid interface velocity–undercooling' relationship exhibiting the well-known bell-shaped kinetic curve. The traveling wave solution of the kinetic PF model as well as the hodograph equation of the solid-liquid interface quantitatively describe the 'velocity–undercooling' relationship obtained in the MD simulation in the whole range of investigated temperatures for melting and growth of $Al_{50}Ni_{50}$ crystals.

Keywords: molecular dynamics, phase field, melting, solidification

(Some figures may appear in colour only in the online journal)

* Dedicated to the blessed memory of Professor Dieter Matthias Herlach who made a study of rapid solidification qualitatively clear and quantitatively accessible.
** Author to whom any correspondence should be addressed.

Original Content from this work may be used under the terms of the Creative Commons Attribution 4.0 licence. Any further distribution of this work must maintain attribution to the author(s) and the title of the work, journal citation and DOI.

© 2022 The Author(s). Published by IOP Publishing Ltd

1. Introduction

Al–Ni alloys are typical multi-phase alloys that easily may exhibit different phases for the same chemical composition but depend on the degree of undercooling. Particularly, a search for disordered phases was carried out in which the main attention in the study was paid to the transition from an ordered to a disordered phase of an intermetallic compound of $Al_{50}Ni_{50}$ composition [1, 2]. Peculiarities of solidification/melting kinetics together with the order–disorder transition were intensively studied experimentally [3–6], at the atomic level by molecular dynamics (MDs) simulation [7–9], and at the mesoscopically spatial level using the phase field (PF) method [10, 11] as well as applying the sharp interface model [12, 13].

In the present work, we revise the comparison of atomistic and mesoscopic theoretical modeling with the application of MDs and PF methods for kinetics of melting and growth of $Al_{50}Ni_{50}$ alloying crystals. Such a comparison has already been done in the previous work [11], however, here we essentially refine calculations to make accessible data of simulation much correct by the following reasons.

(a) The first embedded atom method (EAM) potential for the Ni–Al alloy was proposed by Mishin *et al* [14]. Using this potential the melting temperature of the alloy $Al_{50}Ni_{50}$ was estimated as $T_m = 1520$ K by Kerrache *et al* [8] and later as $T_m = 1545$ K by Kuhn and Horbach [15]. Both estimations of T_m are much smaller than the known experimental value $T_m = 1911$ K [16, 17]. Later, Purja Pun and Mishin [18] developed a new EAM potential for the system Ni–Al which according to our simulations has a melting temperature of $T_m = 1816$ K that is much closer to the experimental data. In comparison to the experimental data the density of the liquid phase is also better described by the later potential.

(b) Based on the first potential of Mishin *et al* [14], the relation between the interfacial growth velocity with temperature of the alloy $Al_{50}Ni_{50}$ was studied by MD simulations using the free solidification method (FSM) [19–21]. Kerrache *et al* [8] estimated the kinetic growth coefficient of the crystalline orientation (100) of $Al_{50}Ni_{50}$ as $\mu_{\langle 100\rangle} = 0.0025\,\mathrm{m\,(s{\cdot}K)^{-1}}$. Using the same potential Kuhn and Horbach [15] in a later study found that the kinetic growth coefficient is much larger $\mu_{\langle 100\rangle} \approx 0.014\,\mathrm{m\,(s{\cdot}K)^{-1}}$. Using the new EAM potential for Ni–Al of Purja Pun and Mishin [18] and Yang *et al* [22] calculated interfacial growth velocities for the (100) and (110) crystalline orientation of $Al_{50}Ni_{50}$ with values of μ of about $0.05\,\mathrm{m\,(s{\cdot}K)^{-1}}$ while in the present work it is found for the same potential that $\mu_{\langle 100\rangle} = 0.0454\,\mathrm{m\,(s{\cdot}K)^{-1}}$.

Due to the above (a) and (b) reasons, we revise MD simulation for the $Al_{50}Ni_{50}$ alloy using the model of Purja Pun and Mishin [18] as a basic model. Upon the revision, the MD-data on crystallization and melting kinetics are further compared with predictions of the kinetic PF model.

The article is organized as follows. Section 2 characterizes material's properties (density, enthalpy, and self-diffusion) in bulk solid and liquid phases of the $Al_{50}Ni_{50}$ alloy which have been obtained by MD-method. Analysis of the velocity predicted by the diffusion-limited theory (DLT) and the kinetic PF model in comparison with the MD-data are presented in section 3. In this comparison, the material's parameters extracted from MD simulation (melting temperature, spacing between crystalline layers, atomic displacement associated with ordering, enthalpy of fusion, activation energy for the atoms diffusion, etc) are used for both theories. A discussion on crystal growth and melting is given in section 4 where the dynamics of PF and its equilibrium state are considered in comparison with the obtained MD-data. Section 5 summarizes our outcomes proving necessity to re-consider and revise MD-data on crystallization and melting kinetics with the developed kinetic PF model.

2. Characterization of bulk phases

The properties of the system $Al_{50}Ni_{50}$ are estimated by means of MD simulations using own code developed in CUDA C language for parallel simulation on graphic processing units. The EAM potential is used to describe the interactions between atoms. The potential energy of an atom i is given by the sum of two contributions

$$U_i = F_i(\rho_i^{\mathrm{h}}) + \frac{1}{2}\sum_j \Phi_{ij}(r_{ij}) \tag{1}$$

the embedding energy F_i, which is a functional of the host electron density ρ_i^{h}, and the sum of effective pair potentials Φ_{ij}. In the EAM the host electron density is simply the sum of the atomic electron densities

$$\rho_i^{\mathrm{h}} = \sum_j \rho_i^{\mathrm{at}}(r_{ij}). \tag{2}$$

For the system Ni–Al the functions F_{Al}, F_{Ni}, $\rho_{\mathrm{Al}}^{\mathrm{at}}$, $\rho_{\mathrm{Ni}}^{\mathrm{at}}$, $\Phi_{\mathrm{Al-Al}}$, $\Phi_{\mathrm{Ni-Ni}}$ and $\Phi_{\mathrm{Ni-Al}}$ of the potential of Purja Pun and Mishin [18] can be found in tabular form in the Interatomic Potentials Repository of the National Institute of Standards and Technology [23].

The densities and enthalpies of the bulk crystalline (bcc) and liquid phases of $Ni_{50}Al_{50}$ were determined from sequences of simulations at constant pressure and temperature (*NpT* runs) using $2 \times 16 \times 16 \times 16$ atoms. Periodic boundary conditions were applied in all directions. The equations of motion were integrated with the velocity-Verlet algorithm with a time step of 1 fs. The Berendsen barostat was used to control pressure and the velocity scaling method to control temperature. The properties of the crystalline B2-NiAl phase were determined along a heating curve at zero pressure and temperatures between 1200 K and 2500 K with temperature steps of 1 K. The sequence started from a B2-NiAl crystal with a density $5.3\,\mathrm{g\,cm^{-3}}$ and particle velocities assigned according to a Maxwell–Bolztmann distribution at 1200 K. The system was equilibrated during 50 ps and simulated another 50 ps to obtain averages of density and enthalpy. Then the temperature was increased and the same procedure was repeated. At the beginning of each simulation new particle velocities were assigned.

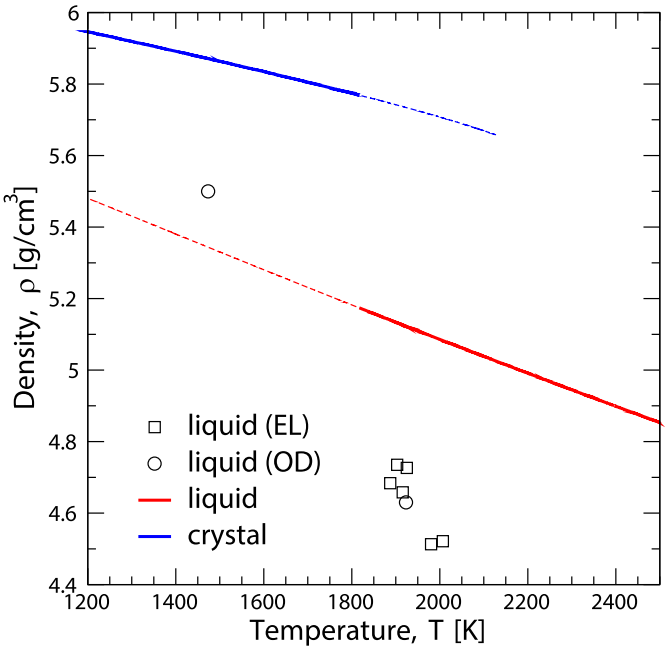

Figure 1. Density $\rho(T)$ of the crystalline and liquid phases of $Al_{50}Ni_{50}$. Results of MD simulation is shown in lines; solid and liquid stable phases are represented by thick lines and metastable phases by thin dashed lines. Symbols correspond to experimental data of Plevachuk *et al* [24] for the liquid phase. Data from electromagnetic levitation (EL) experiments is shown with circles and from optical dilatometry (OD) with squares.

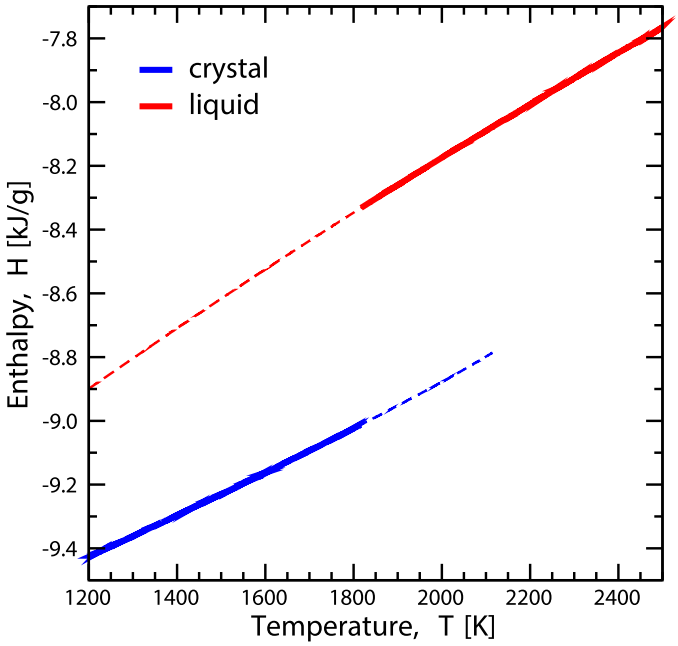

Figure 2. Enthalpy $H(T)$ of the crystalline and liquid phases of $Al_{50}Ni_{50}$ obtained from MD simulations using the EAM potential of Purja Pun *et al* [18]. The thick dashed lines indicate the regions where solid and liquid phases are stable, the thin dashed lines correspond to the metastable phases.

The crystalline phase melts at a temperature above 2100 K (see figure 1), which is much higher than the coexistence temperature of the B2-NiAl at zero pressure for this potential (1816 K). The properties of the liquid phase were determined using the same procedure, but this time along a cooling curve, starting from the stable liquid at 2500 K. The density of the stable crystal and liquid phases are well described by the equations

$$\rho_s(T) = 6.154\,95 - 1.024\,86 \times 10^{-4}T - 6.0772 \times 10^{-8}T^2 \quad (3)$$

$$\rho_l(T) = 6.127\,28 - 5.641\,09 \times 10^{-4}T + 2.174\,07 \times 10^{-8}T^2 \quad (4)$$

where the density ρ is given in g·cm^{-3} and the temperature T in Kelvin.

Figure 1 shows that the values of liquid phase density from MD-simulation compares well with experimental data close to the melting temperature T_m. However, the experimental thermal expansion coefficient seems to be larger than in simulations, i.e. $(d\rho/dT)_{EXP} > (d\rho/dT)_{MD}$. The same behavior has been observed previously for Ni in the comparison of experimental data with simulation results using different EAM potentials [21].

The enthalpies of the stable B2-NiAl and liquid phases (see figure 2) are well described by the equations

$$H_s(T) = -10\,110.5 + 0.503\,451T + 5.566\,12 \times 10^{-5}T^2 \quad (5)$$

$$H_l(T) = -10\,156.1 + 1.131\,97T - 7.047\,44 \times 10^{-5}T^2. \quad (6)$$

Using these expressions the latent heat of melting $\Delta H_m = H_l - H_s$ is given by

$$\Delta H_m(T) = -45.6 + 0.628\,517T - 1.261\,36 \times 10^{-4}T^2 \quad (7)$$

where the units for H are J·g^{-1} and for T are K. Note that the latent heat of melting decreases from 679.8 J·g^{-1} at 1816 K to 527.0 J·g^{-1} at 1200 K.

The diffusion coefficient of the liquid phase at zero pressure ($p = 0$) and temperatures from 1900 K to 1250 K was determined from a sequence of MD-simulations along a cooling curve using steps of 50 K between simulations. At each temperature the liquid was first prepared in a simulation at constant pressure and temperature (NpT), where the liquid reached its averaged equilibrium density. Then, the system is equilibrated at this equilibrium density at fixed volume and constant temperature (NVT). Finally, the system was simulated in microcanonical ensemble NVE during 5 ns using an integration step of 1 fs. According to the Einstein equation the diffusion coefficient D is related to the averaged mean square displacement of particles $\langle \Delta r^2 \rangle$ as

$$D = \frac{1}{6} \lim_{t \to \infty} \frac{d}{dt} \langle \Delta r^2 \rangle. \quad (8)$$

In this equation the brackets represent an average over the particles and over different time origins. Mean square displacement was obtained at different temperatures from simulations of 5×10^6 time steps using an integration step of

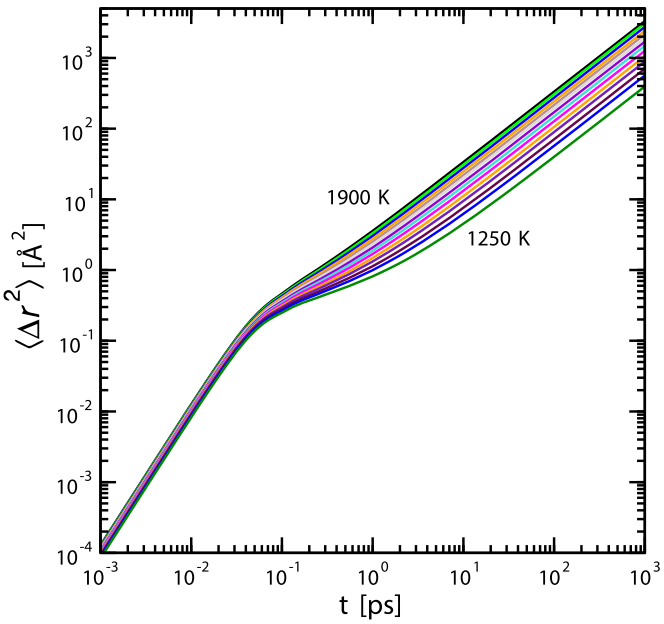

Figure 3. Mean square displacement versus time curves in the liquid phase of $Al_{50}Ni_{50}$ for temperatures between 1900 K and 1250 K obtained from molecular dynamic simulations.

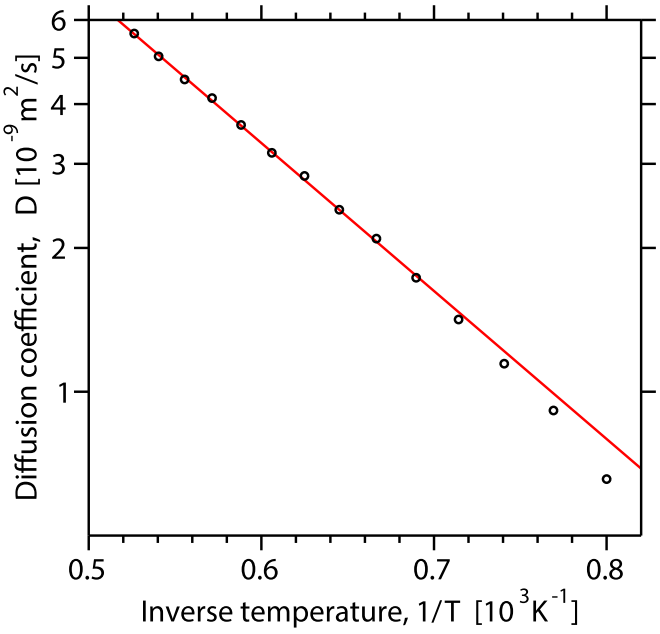

Figure 4. Diffusion coefficient $D(T)$ of the liquid phase of $Al_{50}Ni_{50}$ system obtained from molecular dynamic simulations. The data is represented in an Arrhenius plot and the line corresponds to the fit of the data using equation (12) with materials parameters of table 1.

about 1 fs. Five hundred time origins separated by 10^4 time steps were considered for each simulation. The curves of mean square displacements *versus* time are shown in figure 3 in a double logarithmic plot where the initial ballistic and the late diffusive regimes can be easily identified. The diffusion coefficients calculated from the slope of the curves in the diffusive regime are shown in figure 4. In agreement with the results of Yang *et al* [22], where the same potential has been used, the diffusion coefficient obtained in this work exhibits a deviation from the Arrhenius behavior below 1450 K, however the values are about a factor of 10 higher than in this work.

3. Interfacial velocity in growth and melting of crystals in the $Al_{50}Ni_{50}$ alloy

3.1. Crystal growth from MD simulations

Interfacial growth velocities are estimated by simulations using the FSM. In this method a system made of a crystal, a liquid and an interface separating both is first prepared at the same temperature and pressure (see figure 5). The preparation involves different simulation steps (a) first a crystal is relaxed 50 ps in a simulation at constant pressure and temperature (NpT). (b) Then the averaged simulation box lengths are determined in an NpT run of 50 ps. (c) After this a crystalline and a liquid region are defined. The width of the crystalline region is one third of the simulation box length transversal to growth. The liquid region is melted in a simulation at constant pressure, temperature and area transversal to growth ($NpAT$) at 2500 K during 0.5 ns. In this step the atoms in the crystalline region are kept at fixed positions. (d) In the last preparation step the liquid is cooled down to the initial temperature in a short $NpAT$ simulation of 20 ps. After these preparation steps all the atoms are allowed to move and the system is simulated at constant pressure, temperature and area transversal to growth ($NpAT$ conditions). At the given thermodynamic conditions the stable phase growth in the other unstable phase with a velocity V that can be estimated from the evolution of the simulation box length transversal to growth, L_z. The relation between V and L_z is obtained from the mass balance $dm/dt = 0$ with $m = m_s + m_l$ the total mass, $m_s \approx \rho_s A L_s$ and $m_l \approx \rho_l A L_l$ the mass of the crystal and liquid, respectively. Therefore, considering that $V = 0.5 dL_s/dt$ and $dm_s/dt = -dm_l/dt$ the growth velocity is

$$V = -\frac{\rho_l}{2(\rho_s - \rho_l)} \frac{dL_z}{dt}. \tag{9}$$

In pure systems and congruently melting alloys, such as $Al_{50}Ni_{50}$, stationary crystal growth occurs at constant interfacial velocity, i.e. the simulation box length L_z changes linearly in time. Here, the growth of crystalline $Ni_{50}Al_{50}$ on the melt was studied by simulations at zero pressure and temperatures between 1200 K and 1900 K. The geometry of the initial crystal consists of 12×12×192 B2-NiAl unit cells, i.e. 55 296 atoms. The equations of motion were integrated with the velocity-Verlet algorithm with a integration step of 1 fs. Periodic boundary conditions were applied in all directions. At each temperature, the interfacial growth velocity was computed from the average of dL_z/dt of five independent simulations. The time interval of stationary growth in each of these simulations was 1.5 ns. The pressure was controlled by the Berendsen barostat and the temperature by assigning new velocities to all particles from a Maxwell–Boltzmann distribution every $n_T = 1500$ steps. In this method the total momentum of the system is conserved. The coupling to the thermostat is

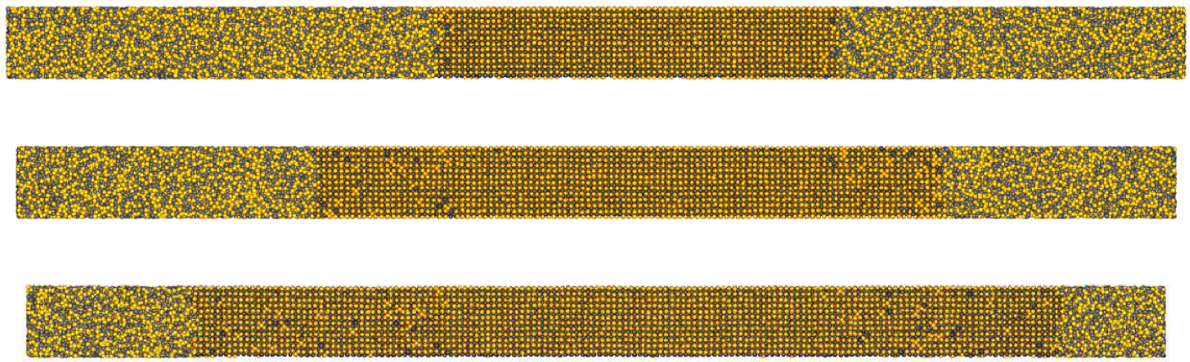

Figure 5. Snapshots of the simulation of crystal growth of $Al_{50}Ni_{50}$ at 1600 K after 0.10 ns (top), 0.70 ns (middle) and 1.4 ns (bottom). The system shrinks on the direction of growth as the crystal, the phase with higher density, advances in to the liquid.

not trivial, previous simulation studies using different thermostats indicate that the interfacial growth velocity depends on the choice of the thermostat parameter [25, 26]. Monk *et al* [25] estimated the kinetic growth coefficient of Ni using the FSM with the layered thermostat method, where the system is divided in several sub-regions, aligned normal to the crystallization direction, that are independently thermostated. In this study it has been found that the growth velocity depends on the choice of the width of the layers, but reach a convergent value for a layer width below 20 Å. In another study the kinetic growth coefficients of an EAM potential of Ti was estimated from the FSM [26] by assigning new velocities to all particles each n_T steps. It has been found that the velocity reaches a convergent value for $n_T > 1000$ steps. In both studies the values of the kinetic growth coefficient found were consistent with the estimation based on the relaxation times of the height correlations of the crystal-liquid interface at coexistence, simulations where no thermostat is needed. In our simulations here we used the same thermostat as in [26] and found that the growth velocity converge for values of $n_T > 1000$ steps. Particularly, comparison of our velocity-temperature MD-data for the orientation 100 using the model of Purja Pun and Mishin [18] shows a good agreement with the results of Yang *et al* [22] at low undercooling but differ at high undercooling, the maximum velocity is about 16 m s^{-1} in the work of Yang *et al* and here 11.33 m s^{-1}.

3.2. Prediction of the DLT

For quantitative description of the interface kinetics and the interface velocity, the DLT by Wilson and Frenkel [27, 28] and the collision-limited theory (CLT) by Turnbull *et al* [19, 29] have been proposed. Depending on the sort of particles and the conditions for their attachment/detachment to/from the interface, these two theories satisfactorily describe the interface velocity with a relatively small driving force, i.e. with relatively small values of undercooling/overheating. Indeed, experimental data and data of atomistic modeling show the existence of a good quantitative description in the narrow temperature range around the melting point where the interface velocity linearly depends on overheating/undercooling [30–32].

With the increase of the driving force, the predictions of DLT and CLT clearly contradict the data of atomistic modeling [33]. The quantitative disagreement of DLT and CLT occurs in the temperature range where the interface velocity exhibits non-linearity depending on increased undercooling at the interface [8, 22]. This non-linearity has the dependence of velocity with saturation [34] or exhibiting the velocity with a maximum at a fixed undercooling [35]. In this section, we compare the temperature-dependent velocity obtained in the present MD simulation with the prediction of DLT [27, 28].

The velocity of solid–liquid interface depends on the Gibbs free energy change on transformation ΔG given by

$$\Delta G = G_{\rm s}(T,C) - G_{\rm l}(T,C) \begin{cases} < 0, & \text{solidification} \\ > 0, & \text{melting} \end{cases} \tag{10}$$

where $G_{\rm l}(T,C,\phi)$ and $G_{\rm s}(T,C,\phi)$ are the Gibbs free energies of the liquid and solid phases, respectively. Then, the DLT-equation for the solid-liquid interface velocity V is described by [27, 28]

$$V = \frac{6a}{\lambda^2} f_0 D(T) \left[1 - \exp\left(\frac{\Delta G}{k_{\rm B}T}\right)\right] \tag{11}$$

with $k_{\rm B} = 8.617 \times 10^{-5}$ eV· K^{-1} the Boltzmann constant and $D(T)$ the liquid diffusion coefficient defined by the thermally-activated law of the Arrhenius-type

$$D(T) = D_0 \exp(-Q/k_{\rm B}T). \tag{12}$$

All parameters and notations from equations (11) and (12) are defined in table 1 to transfer from Gibbs free energy difference ΔG to the undercooling using a simplest expression for the driving force [36]

$$\Delta G = \Delta H_{\rm f}(-\Delta T)/T_{\rm m}, \quad \Delta T = T_{\rm m} - T \tag{13}$$

where ΔT is the undercooling which is necessary for non-zero attachment/detachment of atoms at/from the solid–liquid interface in the case of crystallization/melting. This undercooling is defined as the 'kinetic undercooling' in the dendrite growth models as one of contributions into the total (experimentally measurable) undercooling balance (see [5, 6] and references therein).

Table 1. Materials parameters for congruently melting $Al_{50}Ni_{50}$ alloy used in calculations by diffusion-limited theory (DLT) of growth and melting using the data of present MD simulation.

Parameter	Value
Melting temperature, T_m (K)	1816
Spacing between crystalline layers, a (m)	1.46×10^{-10}
Fraction of collisions with the crystal[a], f_0 (—)	0.8
Atomic displacement associated with ordering, λ (m)	2.40×10^{-10}
Enthalpy of fusion, ΔH (eV·atom^{-1})	0.302
Diffusion prefactor, D_0 (m$^2 \cdot$ s^{-1})	2.424×10^{-7}
Activation energy for diffusion of atoms in the liquid, Q (eV·atom^{-1})	0.6166

[a] The value $6f_0$ used in equation (11) corresponds to the constant C given by Yang *et al* [22]. Indeed, as better fitting, we found the value $f_0 = 0.8$ which gives $C = 4.8$ that is about the value 5.3 obtained by Yang *et al*.

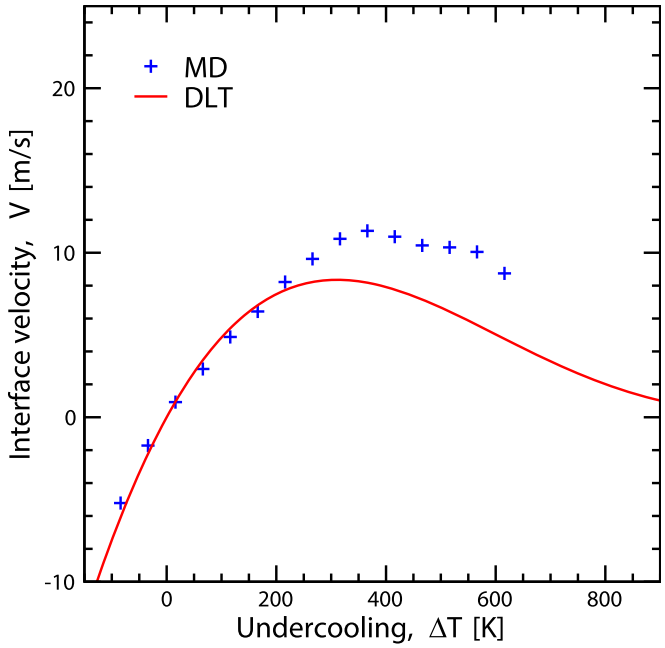

Figure 6. Solid-liquid interface velocity V obtained from MD simulation (+) for the ⟨100⟩-direction of crystals in congruently melting $Al_{50}Ni_{50}$ alloying system. Positive values of the velocity, $V > 0$, present the growth from the undercooled melt with $\Delta T = T_m - T > 0$. Negative values of the velocity, $V < 0$, are consistent with the melting of the overheated crystal having $\Delta T = T_m - T < 0$. The curve presents the DLT-prediction by equation (11) using materials data of table 1.

Equation (11) has been solved together with equations (12) and (13) using parameters of the $Al_{50}Ni_{50}$ alloy from table 1. In this table, the spacing between crystalline layers, a, has been estimated as the half of the unit cell length, i.e. $a = (\bar{\rho}_s)^{-1/3}/2$ with $\bar{\rho}_s$ the number density of the crystal. The atomic displacement associated with ordering has been approximated from MD-data as the first neighbor distance in the liquid phase.

Figure 6 shows the prediction of equation (11) in comparison with the velocities of growth and melting for Al–Ni crystals. A better comparison of DLT-prediction with MD-data has been obtained for the fraction of atomic collisions with the crystal equals $f_0 = 0.8$ (see table 1). However, equation (11) describes MD-data only in the limited range of undercooling (temperature) as it has also been shown previously [32]. Calculations by DLT equation (11) disagree with MD-data of simulation at intermediate and large values of undercooling that is considered as a motivation to find other theoretical predictions being consistent with MD-data.

The example shown in figure 6 is a part of the common crisis of the classic kinetic equations in description of interface movement at arbitrary driving force. Indeed, the DLT [27, 28] and/or CLT [29] well predict experimental data and data of atomistic simulation only around melting point, namely, in the range of $\pm 30 \ldots 150$ K from the melting point (depending of the specific substance or mixture of atoms). Beyond this range both DLT and CLT show clear disagreement with numerous data obtained, for instance, in MD simulations. Here one can mention just a few works [8, 22, 37] where authors directly indicate that DLT and CLT unable to describe MD-data on crystal growth/melting kinetics in a whole range of investigated temperatures close and far from the melting temperature.

The reason of such disagreement is in describing the melting/growth kinetics only by the flux difference between processes of the attachment/detachment of atoms to/from the interface. Now, it is clear that far from the melting temperature the relaxation of kinetic variables also plays essential role that should be taken into account formally in equations for interface motion [38, 39]. Such kinetic variable can, for example, be taken as temporal derivative of the atomic flux. In the PF theory of the elemental substance such kinetic variable is chosen in a form of the gradient flow, i.e. the rate of PF change in time. With taking relaxation of kinetic variables into account the PF is described already by the form of kinetic model.

3.3. The kinetic PF and its parameters

The kinetic PF model is based on the hyperbolic equations including the first and second derivatives of the PF with respect to the time. For one-component elemental system or congruently melting alloys, which solidify without chemical segregation, the kinetic PF model is described by the equation of the hyperbolic type [38, 39]:

$$\tau_\phi \frac{\partial^2 \phi}{\partial t^2} + \frac{\partial \phi}{\partial t} = -\mathcal{M}_\phi \frac{\delta F}{\delta \phi} \qquad (14)$$

where F is the free energy, $\mathcal{M}_\phi$ is the PF mobility, and τ_ϕ is the relaxation time of the gradient flow $\partial\phi/\partial t$, which helps to describe the non-linear behavior of the crystal/liquid interface velocity at large driving forces. The first term of the left-hand side in equation (14) describes relaxation of the gradient flow (acceleration) and the second term there gives the relaxation of the PF itself (velocity). These both relaxations proceed under the driving force $\propto \delta F/\delta\phi$ given by the right-hand side of equation (14). With $\tau_\phi \to 0$, equation (14) transforms to the equation of Mandel'sham and Leontovich [40] which is also known as the time-dependent Ginzburg–Landau equation [41–43] used in the parabolic PF model [44]. The specific form of free energy in equation (14) determines the concrete form of equation. From equation (14), in particular, it is easy to obtain an equation for the propagation of bacteria by the Kolmogorov–Piskunov–Piotrovsky–Fisher equation of diffusion with a delay or an equation for describing the transition from an ordered state to a disordered state by the Allen–Cahn equation.

Due to taken the second time derivative in equation (14) into account, the time scale becomes much refined allowing for analyze processes at short time periods comparable with the freezing of local volumes and, therefore, quantitatively evaluate local non-equilibrium states [39]. These highly non-equilibrium states are solidifying/melting with the fairly exhibiting nonlinearity in the interface velocity as observed experimentally, for instance, in solidification kinetics of glass forming alloys [45].

Quantitative investigations of the kinetic process at the solid/liquid interface require an accurate estimation of the PF parameters for equation (14). Namely $\mathcal{M}_\phi$ and τ_ϕ, should be based on the solid/liquid material properties. Similar to the thin interface analysis of [44], $\mathcal{M}_\phi$ and τ_ϕ is correlated to the anisotropic kinetic coefficient and the crystal-melt interface free energy [46]. The use of MD technique for study of crystal growth, determination of capillary and kinetic properties of the diffuse interface between liquid and solid phases gives ability to obtain the interface mobility $\mathcal{M}_\phi$ and τ_ϕ.

3.4. Prediction of the PF model

The sharp-interface limit of the hyperbolic equation (14) leads the hodograph equation presenting the acceleration-velocity-Gibbs–Thomson-type equation for the isotropic interface [47] and acceleration-velocity-Herring-type equation for the anisotropic interface [48]. These both cases also define the velocity-dependent width of the diffuse interface having the parameter V_ϕ as the maximum PF propagation speed depending on the relaxation time τ_ϕ, such that $V_\phi = (D_\phi/\tau_\phi)^{1/2}$, where D_ϕ is the PF diffusion coefficient[5]. In searching for the hodograph equation, the obtained interface width looks like

$$\ell(V) = \begin{cases} \delta, & \text{if } \mathrm{V} = 0 \\ \delta\left[1 - V^2/V_\phi^2\right]^{1/2}, & \text{if } \mathrm{V} < \mathrm{V}_\phi \\ \to 0, & \text{if } \mathrm{V} \to \mathrm{V}_\phi - 0 \end{cases} \tag{15}$$

where δ is the equilibrium mean interface width. As equation (15) shows, the diffuse interface width ℓ takes a constant value δ in static equilibrium $V = 0$, always different from a constant δ in dynamics $V \neq 0$, and tends to zero with the transition to sharp interface as soon as the interface velocity V approaches the maximum speed V_ϕ for the PF propagation. Such variety in the width ℓ exhibits its physical meaning, favorably distinguishing the expression for the width (15) from the constant for the interface width δ existing always in the analysis of parabolic PF models.

The hodograph equation provides the interface velocity in the steady-state regime, $V = \text{const}$, as function of undercooling ΔT by [47, 48]

$$V = \pm\frac{\mu_{\mathrm{K}}^{\mathrm{PF}}(\Delta T)\Delta T}{\sqrt{1 + \left[\mu_{\mathrm{K}}^{\mathrm{PF}}(\Delta T)\Delta T/V_\phi(\Delta T)\right]^2}}. \tag{16}$$

The crystal growth in solidification is defined by the sign 'plus' and the crystal melting is defined by the sign 'minus'. The interface velocity (16), which follows from the hodograph equation, presents the velocity of the traveling wave in steady state dynamics of the PF profile [49].

In equation (16), the kinetic coefficient $\mu_{\mathrm{K}}^{\mathrm{PF}}$ of the 'solid-liquid' interface motion is the function of the kinetic undercooling ΔT:

$$\mu_{\mathrm{K}}^{\mathrm{PF}}(\Delta T) = \frac{\Delta H_{\mathrm{m}}}{\gamma T_{\mathrm{m}}} D_\phi(\Delta T). \tag{17}$$

The maximum speed of the PF as the function of undercooling is defined by

$$V_\phi(\Delta T) = \sqrt{D_\phi(\Delta T)/\tau_\phi} \tag{18}$$

where the relaxation time τ_ϕ is taken in the present work as a constant, independent of temperature. The diffusion coefficient of the PF in equations (17) and (18) is given by

$$D_\phi = D_\phi^0 \exp\left(-\frac{E_{\mathrm{A}}/k_{\mathrm{B}}}{T_{\mathrm{m}} - \Delta T - T_{\mathrm{A}}}\right). \tag{19}$$

Equation (16) has been solved together with equations (17)–(19) using parameters of the $Al_{50}Ni_{50}$ alloy from table 2. These parameters represent: melting temperature, T_{m}, found for $V = 0$; interface energy, γ, as averaged value of the solid–liquid interfacial tension, this value is taken from the forthcoming paper [50]; enthalpy of fusion, ΔH_{f}, taken at T_{m}. Finally, relaxation time of gradient flow, τ_ϕ, diffusion coefficient of the PF, D_ϕ, diffusion factor of the PF, D_ϕ^0, energetic barrier, $E_{\mathrm{A}}/k_{\mathrm{B}}$, and pseudo-glass temperature, T_{A}, are obtained as the parameters which are fitting MD-data for the interface velocity.

[5] One of the methods to determine the relaxation time τ_ϕ or the maximum speed V_ϕ is related to the determination of the diffuse interface width ℓ as a function of the crystal growth velocity V. Indeed, an innovative MD approach based on the atomistic obtaining of the interface width (15) is integrated with the kinetic phase-field model for quantitative predictions of non-equilibrium crystal growth kinetics [46].

Table 2. Material parameters of the congruently-melting alloy $Al_{50}Ni_{50}$ used for calculation of the traveling wave velocity of the phase field.

Parameter	Set 1[a]	Set 2[b]
Melting temperature, T_m (K)	1816	1816
Interfacial free energy, γ ($J{\cdot}m^{-2}$)	0.2875	0.2875
Enthalpy of fusion, ΔH_f ($J{\cdot}m^{-3}$)	3.9214×10^9	3.9214×10^9
Relaxation time of gradient flow, τ_ϕ (s)	$\to 0$	1.232×10^{-12}
Diffusion coefficient of the phase field, D_ϕ ($m^2 \cdot s^{-1}$)	5.3898×10^{-9}	—
Diffusion factor of the phase field, D^0_ϕ ($m^2 \cdot s^{-1}$)	—	1.095×10^{-8}
Energetic barrier, E_A/k_B (K)	—	525.934
Pseudo-glass temperature, T_A (K)	—	910

[a] Represents the set of parameters for traveling wave solution following from the parabolic phase field equation, i.e. equation (14) with $\tau_\phi = 0$, to calculate the interface velocity (16) with $\tau_\phi \to 0$ and D_ϕ =const.
[b] Represents the set of parameters for traveling wave solution of the hyperbolic phase field equation (14) to calculate the interface velocity by equations (16)–(19).

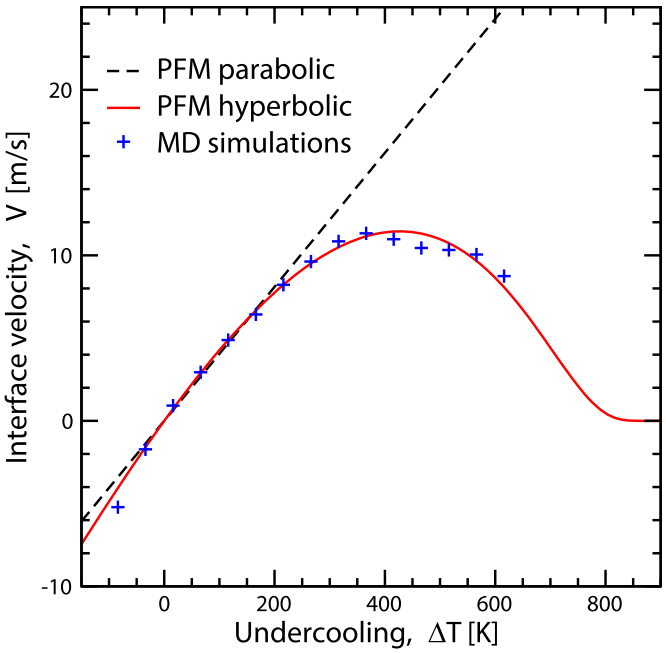

Figure 7. Solid-liquid interface velocity V obtained from MD simulation (+) for the ⟨100⟩-orientation of crystals in congruently melting $Al_{50}Ni_{50}$ alloy. Positive values of the velocity, $V > 0$, present the growth from the undercooled melt with $\Delta T = T_m - T > 0$. Negative values of the velocity, $V < 0$, are consistent with the melting of the overheated crystal having $\Delta T = T_m - T < 0$. The dashed line is obtained by solution of equation (16) using materials data from Set 1 of table 2. The solid curve is given by solution of equation (16) using materials data from Set 2 of table 2.

Figure 7 demonstrates the solution of equation (16) for two cases, which are defined by two sets of parameters for Al–Ni alloy from table 2 and which determine two regimes of PF dynamics. The first mode is determined by the relaxation of the PF by solving equation (16) with zero relaxation time of the gradient flow, $\tau = 0$, i.e. with an infinite propagation speed of the leading edge of the PF, $V_\phi \to \infty$ (see Set 1 in table 2). In this case, the equation (14) becomes parabolic, and the interface velocity (16) is described by the linear law $V \propto \Delta T$ [6]. This mode is shown in figure 7 by a straight line that describes the growth and melting of a crystal in the region around melting temperature $T = T_m$ according to a limited set of MD-data. The second mode of PF relaxation occurs with finite relaxation time τ_ϕ and the finite velocity V_ϕ of the leading edge of the PF (see Set 2 in table 2). Equation (14) in this case becomes hyperbolic with the clear non-linearity in velocity (16). This mode is shown in figure 7 by a curve with a maximum that describes the growth and melting of the crystal over the entire undercooling range in accordance with the full set of MD data obtained for the interface velocity.

4. Discussion

4.1. Growth

As it is seen in figure 7, the crystal growth ends at very high undercooling, $\Delta T \approx 830$ K, which corresponds to the complete cessation of the kinetics of particle attachment to the 'crystal–liquid' interface. Obviously, at large ΔT, the liquid freezes with the cessation of the PF propagation: D_ϕ and V_ϕ tend to zero at $\Delta T \approx 830$ K, see figure 8. The transition to such a frozen state is equivalent to the formation of an amorphous state. This transition occurs continuously, in the crossover mode, judging by the kinetic curves of figures 7 and 8. However, this crossover has a different intensity in its dynamics.

[6] One important feature for the transition to the solution of the parabolic model can be outlined. Namely, with $\tau_\phi \to 0$, i.e. with $V_\phi \to \infty$ for equations (16)–(19), the square root in equation (16) transforms into unity, but the non-equilibrium function D_ϕ, given by equation (19), still stays in the governing system of algebraic equations. Formally, this function D_ϕ is inversely proportional to the viscosity function given by the well-known Vogel–Fulcher–Tammann equation. This viscosity is already not the function of an Arrhenius type, but it is derived from a local nonequilibrium theory consistently with mode-coupling theory [51]. Therefore, the non-equilibrium function (19) cannot remain in the solution of the parabolic model, which is a model based on the hypothesis of local thermodynamic equilibrium. The D_ϕ-function (19) simply transforms to a constant value in the local equilibrium limit. Taking this constant value from Set 1 of table 2 and using it into the solution of the parabolic model, equations (16)–(19) with $\tau_\phi \to 0$, one gets natural result: the interface velocity depends linearly on undercooling, $V \propto \Delta T$, see figure 7.

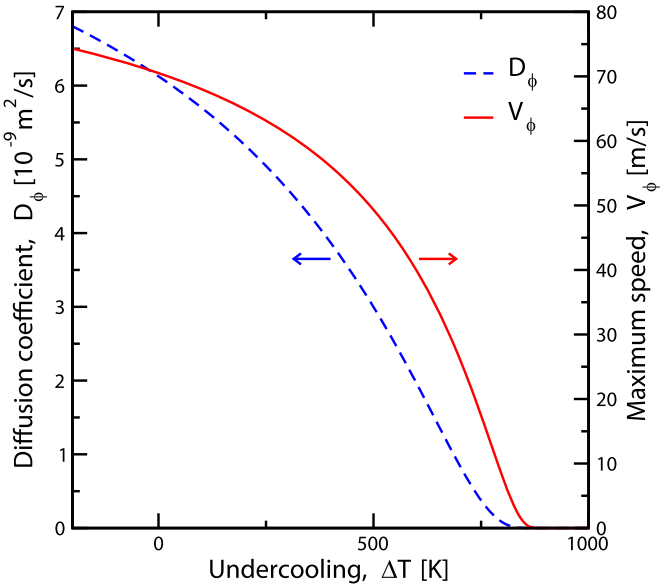

Figure 8. Phase field diffusion coefficient D_ϕ and maximum speed V_ϕ as functions of undercooling $\Delta T = T_\mathrm{m} - T$. V_ϕ and D_ϕ have been computed by equations (18) and (19), respectively, at the value of relaxation time from Set 2 of table 2.

In the interval $400 \lesssim \Delta T(\mathrm{K}) \lesssim 800$, the crossover has more intense dynamics than in the interval $0 < \Delta T(\mathrm{K}) \lesssim 400$. This can be seen from the averaged slopes of the curves for the kinetic parameters D_ϕ and V_ϕ, see figure 8. In this regard, note that around $\Delta T \approx 400$ K:

(a) the maximum of the interface velocity V occurs (see figure 7), i.e. starting from this undercooling, intense freezing of the liquid causes a slowdown in the crystal growth kinetics;
(b) the deviation of the diffusion mobility of atoms from the Arrhenius law begins with the transition to the super-Arrhenius diffusion behavior[7] shown in figure 4, i.e. starting from this undercooling, the intense freezing of the liquid causes an abnormal decrease in the mobility of atoms.

The different intensity of the crossover in freezing the motion of the PF, the slowdown crystal growth kinetics, and deceleration of atomic mobility has so far only a phenomenological statement by the above points (a) and (b). To elucidate the cause of these phenomena, it would be appropriate to carry out an atomic and cluster analysis of the microstructure of the liquid and the diffuse interface between the phases in equilibrium and at various undercoolings in the steady-state mode of crystallization [37, 52, 55].

4.2. Equilibrium

It is interesting to note that the PF has a non-zero maximum speed to establish an equilibrium profile. Figure 8 demonstrates this effect for $\Delta T = 0$: establishing of equilibrium profile proceeds even faster than the propagation of the leading edge of the PF in dynamics with $\Delta T \lessgtr 0$ ($\Delta T > 0$ provides growth and $\Delta T < 0$ leads to the melting of crystals):

$$\text{at equilibrium } V_\phi|_{\Delta T=0} > V_\phi|_{\Delta T \lessgtr 0} \text{ in dynamics.}$$

This can be interpreted in such a way that for the propagation of the leading edge of the PF in dynamics, some additional time is required for the relaxation of the nonzero gradient flow. This reduces the maximum propagation velocity of the PF front in comparison with the maximum velocity of the PF front in equilibrium, where the relaxation of the gradient flow does not exist.

4.3. Difference in crystal's melting and growth

As it is well-known, crystallization and melting represent asymmetric processes relative to the temperature change. This is clearly seen in figures 7 and 8 from which one gets

$$\begin{aligned}\text{melting intensity} &= |-dV/d(\Delta T)|_{\Delta T<0} > dV/d(\Delta T)|_{\Delta T>0} \\ &= \text{growth intensity.}\end{aligned}$$

The difference in intensity of growth and melting of crystals is clearly seen by the slopes of the velocity curves shown in figure 7 at $\Delta T > 0$ (growth) and $\Delta T < 0$ (melting). Because the PF represents the envelope of the maxima of the atomic density amplitudes, the difference in intensity of growth and melting of crystals can also be recollected from the results of modeling of atomic density fields. For example, amplitudes of PF crystals propagate much more intensively in melting dynamics as compared to the crystal growth dynamics of cubic and triangle lattices, see figures 2 and 3 in the work [56]. Such inequality and asymmetry of processes are explained by the fact that less energy is required to destroy atomic bonds (in melting) than it is necessary to create interatomic bonds at the phase interface (for crystallization). Therefore, at the same absolute value of the driving force $|\Delta T|$, the rate of melting becomes higher than the crystal growth rate.

5. Conclusions

The EAM potential of Purja Pun and Mishin [18] was used to study the growth and melting of $Al_{50}Ni_{50}$ crystals by MD simulations. This study included the characterization of the bulk liquid and B2-crystalline phase by the estimation of the crystal-liquid interfacial free energy, the crystal growth/melting velocities and the melting temperature. Our results for the enthalpies, densities, and diffusion coefficient of the melt agree well with the work of Turlo *et al* [57], which made a revision of the bulk properties for the potential of Purja Pun and Mishin [18]. The experimental density of the liquid phase [24] is much better described than in the previous model of Mishin [14]. The novel 'velocity–undercooling/overheating' MD-data obtained from the FSM [19–21] is in fair agreement with data reported in the work

[7] The transition to super-Arrhenius behavior was shown, first, in the experiments and theoretical analysis of liquid viscosity [52–54].

of Yang *et al* [22], where the same potential was used. The interface velocities are similar close to the phases coexistence but differ at higher undercooling. In particular, the maximum interface velocity obtained by Yang *et al* is higher than ours by a factor 1.4. An alternative test of the novel potential used in the present work and exhibited reasonable values of parameters (temperature dependent functions) can be made by extended study using a recently developed machine learning potentials as for an Al–Ni–Cu [58].

The obtained MD-data on melting and growth of $Al_{50}Ni_{50}$-crystals exhibit the well-known curve 'velocity–undercooling/overheating' with the maximum for the growth velocity at fixed undercooling. Because such a bell-shaped MD-curve for the growth velocity is not described quantitatively by the classical DLT of Wilson and Frenkel [27, 28], the kinetic PF model [39, 45] has been used for the analysis of melting and solidification.

The kinetic PF model includes relaxation of the PF to predict the interface velocity as well as relaxation of the gradient flow (the rate of PF change) to describe the effect of interface inertia. Like Newton's equation of motion, the PF equation with acceleration and velocity is allowing to describe slow and fast regimes of interface propagation self-consistently. Specifically, analytical solution of the model in a form of traveling wave of the PF or, equivalently, the hodograph equation of the interface describe well MD-data for the interface velocity in the temperature range presently accessible for the growth and melting of crystals. As a particular peculiarity, the velocity of the PF traveling wave describes the faster melting kinetics compared to the much slower crystal growth process at the same absolute degree of the driving force consistently with the obtained MD-data.

As a final note, as the rapidly solidifying and melting techniques are becoming much popular in modern technologies (from atomization up to selective laser melting techniques), the present kinetic PF model should be actually informed by the material's properties including parameters specifically related to the model such as the time for relaxation of the gradient flow of the PF and the maximum speed for propagation of the leading edge for the PF. Therefore, one of the necessary directions in materials research looks in the advancement of atomistically informed PF models.

Data availability statement

The computational codes and all necessary data are available upon reasonable request from the authors.

Acknowledgment

This work was financially supported by Russian Science Foundation under Project No. 21-19-00279. P K G acknowledges the support from the German Science Foundation (DFG) under the Project GA 1142/11-1. R E R acknowledges financial support from Project ANID FONDECYT 1190101 and from Centro CRHIAM Project ANID/FONDAP/15130015

ORCID iDs

Roberto E Rozas https://orcid.org/0000-0002-6466-5162
Vladimir Ankudinov https://orcid.org/0000-0001-8563-5862
Peter K Galenko https://orcid.org/0000-0003-2941-7742

References

[1] Greer A L and Assadi H 1997 Rapid solidification of intermetallic compounds *Mater. Sci. Eng.* A **226–228** 133–41
[2] Assadi H, Oghabi M and Herlach D M 2009 Influence of ordering kinetics on dendritic growth morphology *Acta Mater.* **57** 1639–47
[3] Assadi H, Reutzel S and Herlach D M 2006 Kinetics of solidification of B2 intermetallic phase in the Ni–Al system *Acta Mater.* **54** 2793
[4] Reutzel S, Hartmann H, Galenko P K, Schneider S and Herlach D M 2007 Change of the kinetics of solidification and microstructure formation induced by convection in the Ni–Al system *Appl. Phys. Lett.* **91** 0419113
[5] Herlach D M, Binder S, Galenko P K, Gegner J, Holland-Moritz D, Klein S, Kolbe M and Volkmann T 2015 Containerless undercooled melts: ordering, nucleation and dendrite growth *Metall. Mater. Trans.* A **46** 4921–36
[6] Herlach D M, Burggraf S, Galenko P K, Gandin C-A, Garcia-Escorial A, Henain H, Karrasch C, Mullis A, Rettenmayr M and Valloton J 2017 Solidification of undercooled melts of Al-based alloys on Earth and in space *JOM* **69** 1303–10
[7] Tang C and Harrowell P 2013 Anomalously slow crystal growth of the glass-forming alloy CuZr *Nat. Mater.* **12** 507–11
[8] Kerrache A, Horbach J and Binder K 2008 Molecular-dynamics computer simulation of crystal growth and melting in $Al_{50}Ni_{50}$ *Europhys. Lett.* **81** 58001
[9] Zhang X Q, Yang Y, Gao Y F, Hoyt J J, Asta M and Sun D Y 2012 Disorder trapping during crystallization of the B2-ordered NiAl compound *Phys. Rev.* E **85** 041601
[10] Assadi H 2007 A phase-field model for non-equilibrium solidification of intermetallics *Acta Mater.* **55** 5225–35
[11] Galenko P K, Salhoumi A and Ankudinov V 2019 Kinetics of rapid crystal growth: phase field theory versus atomistic simulations *IOP Conf. Ser.: Mater. Sci. Eng.* **529** 012035
[12] Boettinger W J and Aziz M J 1989 Theory for the trapping of disorder and solute in intermetallic phases by rapid solidification *Acta Metall.* **37** 3379–91
[13] Hartmann H, Holland-Moritz D, Galenko P K and Herlach D M 2009 Evidence of the transition from ordered to disordered growth during rapid solidification of an intermetallic phase *Europhys. Lett.* **87** 40007
[14] Mishin Y, Mehl M J and Papaconstantopoulos D A 2002 Embedded-atom potential for B2–NiAl *Phys. Rev.* B **65** 224114
[15] Kuhn P and Horbach J 2013 Molecular dynamics simulation of crystal growth in $Al_{50}Ni_{50}$: the generation of defects *Phys. Rev.* B **87** 014105
[16] Singleton M F, Murray J L and Nash P 1986 *Al–Ni Binary Alloy Phase Diagrams* ed T B Massalski (Metals Park, OH: American Society for Metals) pp 181–4
[17] Okamoto H 2004 Al–Ni (Aluminum-Nickel) *J. Phase Equilib. Diffus.* **25** 394
[18] Purja Pun G P and Mishin Y 2009 Development of an interatomic potential for the Ni-Al EAM model *Phil. Mag.* **89** 3245–67

[19] Broughton J Q, Gilmer G H and Jackson K A 1982 Crystallization rates of a Lennard-Jones liquid *Phys. Rev. Lett.* **49** 1496

[20] Sun D Y, Asta M and Hoyt J J 2004 Kinetic coefficient of Ni solid–liquid interfaces from molecular-dynamics simulations *Phys. Rev.* B **69** 024108

[21] Rozas R E, Demirag A D, Toledo P G and Horbach J 2016 Thermophysical properties of liquid Ni around the melting temperature from molecular dynamics simulation *J. Chem. Phys.* **145** 064515

[22] Yang Q, Liu H and Peng H 2021 Crystal growth in deeply undercooled $Ni_{50}Al_{50}$: signature of the ordering sequence at the interface *J. Chem. Phys.* **154** 194503

[23] Interatomic Potentials Repository of the National Institute of Standards and Technology (available at: www.ctcms.nist.gov/potentials/system/Al-Ni/)

[24] Plevachuk Y, Egry I, Brillo J, Holland-Moritz D and Kaban I 2007 Density and atomic volume in Al-Fe and Al–Ni binary alloys *Int. J. Mater. Res.* **98** 107–1

[25] Monk J, Yang Y, Mendelev M I, Asta M, Hoyt J J and Sun D Y 2010 Determination of the crystal-melt interface kinetic coefficient from molecular dynamics simulations *Modelling Simul. Mater. Sci. Eng.* **18** 015004

[26] Rozas R E, MacDowell L G, Toledo P G and Horbach J 2021 Crystal growth of bcc titanium from the melt and interfacial properties: a molecular dynamics simulation study *J. Chem. Phys.* **154** 184704

[27] Wilson H W 1900 On the velocity of solidification and viscosity of super-cooled liquids *London, Edinburgh Dublin Phil. Mag. J. Sci.* **50** 238–50

[28] Frenkel J 1946 *Kinetic Theory of Liquids* (New York: Oxford University Press)

[29] Turnbull D 1962 On the relation between crystallization rate and liquid structure *J. Phys. Chem.* **66** 609–13

[30] Borisov V T 1987 *Theory of the Two-Phase Region of a Metallic Ingot* (Moscow: Metallurgiya)

[31] Mendelev M I, Rahman M J, Hoyt J J and Asta M 2010 Molecular-dynamics study of solid-liquid interface migration in fcc metals *Modelling Simul. Mater. Sci. Eng.* **18** 074002

[32] Salhoumi A and Galenko P K 2017 Analysis of kinetics: Gibbs-Thomson equation and of kinetic rate theory *IOP Conf. Ser.: Mater. Sci. Eng.* **192** 012014

[33] Ashkenazy Y and Averback R S 2007 Atomic mechanisms controlling crystallization behaviour in metals at deep undercoolings *Europhys. Lett.* **79** 26005

[34] Hoyt J J, Sadigh B, Asta M and Foiles S M 1999 Kinetic phase field parameters for the Cu-Ni system derived from atomistic computations *Acta Mater.* **47** 3181–7

[35] Chan W L, Averback R S, Cahill D G and Ashkenazy Y 2009 Solidification velocities in deeply undercooled silver *Phys. Rev. Lett.* **102** 095701

[36] Thompson C V and Spaepen F 1979 On the approximation of the free energy change on crystallization *Acta Metall.* **27** 1855–9

[37] Sun G, Xu J and Harrowell P 2018 The mechanism of the ultrafast crystal growth of pure metals from their melts *Nat. Mater.* **17** 881–6

[38] Galenko P and Jou D 2005 Diffuse-interface model for rapid phase transformations in nonequilibrium systems *Phys. Rev.* E **71** 046125

[39] Galenko P K and Jou D 2019 Rapid solidification as non-ergodic phenomenon *Phys. Rep.* **818** 1–70

[40] Mandel'shtam L I and Leontovich M A 1937 On the theory of absorption of sound in liquids *Zh. Eksp. Teor. Fiz., [Sov. Phys. JETP]* **7** 438–49

[41] Ginzburg V L and Landau L D 1950 On the theory of superconductivity *Zh. Eksp. Teor. Fiz. [Sov. Phys. JETP]* **20** 1064–87

[42] Landau L D and Khalatnikov I M 1954 *Dokladii Academii Nauk CCCP* vol 96 p 469

[43] Lifshitz E M and Pitaevskii L P 1981 *Physical Kinetics* (Elmsford, NY: Pergamon Press)

[44] Echebarria B, Folch R, Karma A and Plapp M 2004 Quantitative phase-field model of alloy solidification *Phys. Rev.* E **70** 061604

[45] Galenko P K, Ankudinov V, Reuther K, Rettenmayr M, Salhoumi A and Kharanzhevskiy E V 2019 Thermodynamics of rapid solidification and crystal growth kinetics in glass forming alloys *Phil. Trans.* A **377** 20180205

[46] Kavousi S, Ankudinov V, Galenko P K and Zaeem A M 2022 Atomistically informed kinetic phase field modeling of non-equilibrium crystal growth during rapid solidification *Acta Mater.* submitted

[47] Salhoumi A and Galenko P K 2016 Gibbs-Thomson condition for the rapidly moving interface in a binary system *Phys.* A **447** 161–71

[48] Galenko P K and Salhoumi A 2021 The hodograph equation for slow and fast anisotropic interface propagation *Phil. Trans. R. Soc.* A **379** 20200324

[49] Galenko P K and Ankudinov V 2019 Local non-equilibrium effect on the growth kinetics of crystals *Acta Mater.* **168** 203–9

[50] Rozas R E, Salazar L A and Horbach J 2022 Interfacial properties and crystal growth of Ni and Ni50Al50 from molecular dynamics simulations *J. Appl. Phys.*

[51] Vasin M G and Vinokur V M 2019 Description of glass transition kinetics in 3D XY model in terms of gauge field theory *Physica* A **525** 1161–9

[52] Soklaski R, Nussinov Z, Markow Z, Kelton K F and Yang L 2013 Connectivity of icosahedral network and a dramatically growing static length scale in Cu-Zr binary metallic glasses *Phys. Rev.* B **87** 184203

[53] Blodgett M E, Egami T, Nussinov Z and Kelton K F 2015 Proposal for universality in the viscosity of metallic liquids *Sci. Rep.* **5** 13837

[54] Jaiswal A, Egami T, Kelton K F, Schweizer K S and Zhang Y 2016 Correlation between fragility and the Arrhenius crossover phenomenon in metallic, molecular and network liquids *Phys. Rev. Lett.* **117** 205701

[55] Galenko P K, Wonneberger R, Koch S, Ankudinov V, Kharanzhevskiy E V and Rettenmayr M 2020 Bell-shaped "dendrite velocity-undercooling" relationship with an abrupt drop of solidification kinetics in glass forming Cu-Zr(-Ni) melts *J. Cryst. Growth* **532** 125411

[56] Ankudinov V, Elder K R and Galenko P K 2020 Traveling waves of the solidification and melting of cubic crystal lattices *Phys. Rev.* E **102** 062802

[57] Turlo V, Baras F and Politano O 2017 Comparative study of embedded-atom methods applied to the reactivity in the Ni–Al system *Modelling Simul. Mater. Sci. Eng.* **25** 064002

[58] Ryltsev R E and Chtchelkatchev N M 2022 Deep machine learning potentials for multicomponent metallic melts: development, predictability and compositional transferability *J. Mol. Liq.* **349** 118181